NANO LETTERS

Letter

pubs.acs.org/NanoLett

Strong Two-Photon-Induced Fluorescence from Photostable, Biocompatible Nitrogen-Doped Graphene Quantum Dots for Cellular and Deep-Tissue Imaging

Qian Liu, Beidou Guo, Ziyu Rao, Baohong Zhang, and Jian Ru Gong*

National Center for Nanoscience and Technology, 11 Zhongguancun Beiyitiao, Beijing 100190, China

Supporting Information

ABSTRACT: Bright two-photon fluorescent probes are highly desirable to be able to optically probe biological activities deep inside living organisms with larger imaging depth, minor autofluorescence background, and less photodamage. In this study, we report the biocompatible nitrogen-doped graphene quantum dots (N-GQDs) as efficient two-photon fluorescent probes for cellular and deep-tissue imaging. The N-GQD was prepared by a facile solvothermal method using dimethylformamide as a solvent and nitrogen source. The two-photon absorption cross-section of N-GQD reaches 48 000 Göppert-Mayer units, which far surpasses that of the organic dyes and is comparable to that of the high performance semiconductor QDs, achieving the highest value ever reported for carbon-based nanomaterials. More importantly, a study of penetration depth in tissue phantom demonstrates that the N-GQD can achieve a large imaging depth of 1800 μm, significantly extending the fundamental two-photon imaging depth limit. In addition, the N-GQD is nontoxic to living cells and exhibits super photostability under repeated laser irradiation. The high two-photon absorption cross-section, large imaging depth, good biocompatibility, and extraordinary photostability render the N-GQD an attractive alternative probe for efficient two-photon imaging in biological and biomedical applications.

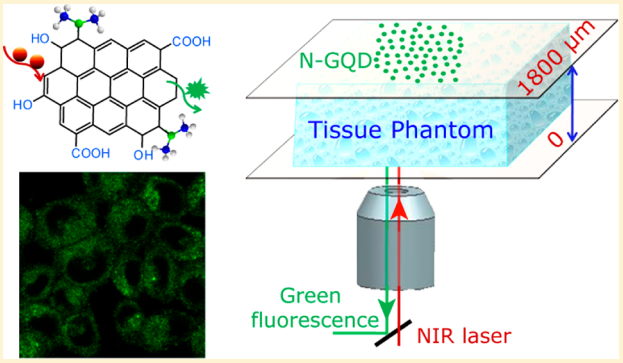

KEYWORDS: *Two-photon fluorescence, bioimaging, deep-tissue, nitrogen-doped, graphene quantum dots, imaging depth*

Two-photon fluorescence imaging (TPFI) with advantages such as a larger penetration depth, minimized tissue autofluorescence background, and reduced photodamage in biotissues has received much attention for its promising applications in both basic biological research and clinical diagnostics.[1,2] Advances in two-photon microscope further demonstrate the possibility of TPFI as a powerful technique to probe deep inside various organ tissues of living organisms via a noninvasive way.[3,4] Nevertheless, many applications in scattering deep tissues are currently handicapped by the fundamental imaging depth limit (~1000 μm) due to a lack of two-photon fluorescent probes with enough brightness.[5,6] In the past decades, organic dyes and semiconductor quantum dots (QDs) are widely studied two-photon probes.[7−10] But the rapid photobleaching effect and limited two-photon absorption cross-section of organic dyes hamper the imaging depth. The serious toxicity of heavy metals in semiconductor QDs causes concern for in vivo bioimaging, despite of their strong two-photon fluorescence. Therefore, the availability of bright fluorescent probes with large two-photon absorption cross sections as well as good biocompatibility is still a critical challenge for deep-tissue TPFI.

Recently, fluorescent carbon-based nanomaterials, including carbon dots (C-Dots), graphene oxide (GO) nanoparticles, and the emerging graphene quantum dots (GQDs) are attracting increasing interest in the field of bioimaging for their good biocompatibility and photostability.[11−15] Sun et al. reported the multiphoton imaging of surface-passivated C-Dots with a higher two-photon absorption cross section of 39 000 Göppert-Mayer units (GM).[16] The two-photon fluorescence of polyethylene glycol linked GO nanoparticle with a size of ~30 nm was applied to in vitro and in vivo bioimaging, obtaining an imaging depth of 300 μm.[17,18] Two-photon imaging using the GQD has also been reported for cell labeling.[19] The quasi zero-dimensional GQD with a single atomic layer gives rise to several advantages over other carbon-based nanomaterials for potential deep-tissue TPFI. First, the bandgap and fluorescence of GQDs can be effectively tuned by doping hetero atoms to the π-conjugated system.[20−24] A blue shift in fluorescence emission has been reported for GQDs after doped with nitrogen atom through an electrochemical method due to the strong electron-withdrawing effect of the doped nitrogen.[20] It can be expected that doping nitrogen through introducing strong electron-donating groups such as dimethylamido could result in a red shift of fluorescence and achieve

Received: January 28, 2013
Revised: March 21, 2013
Published: May 15, 2013

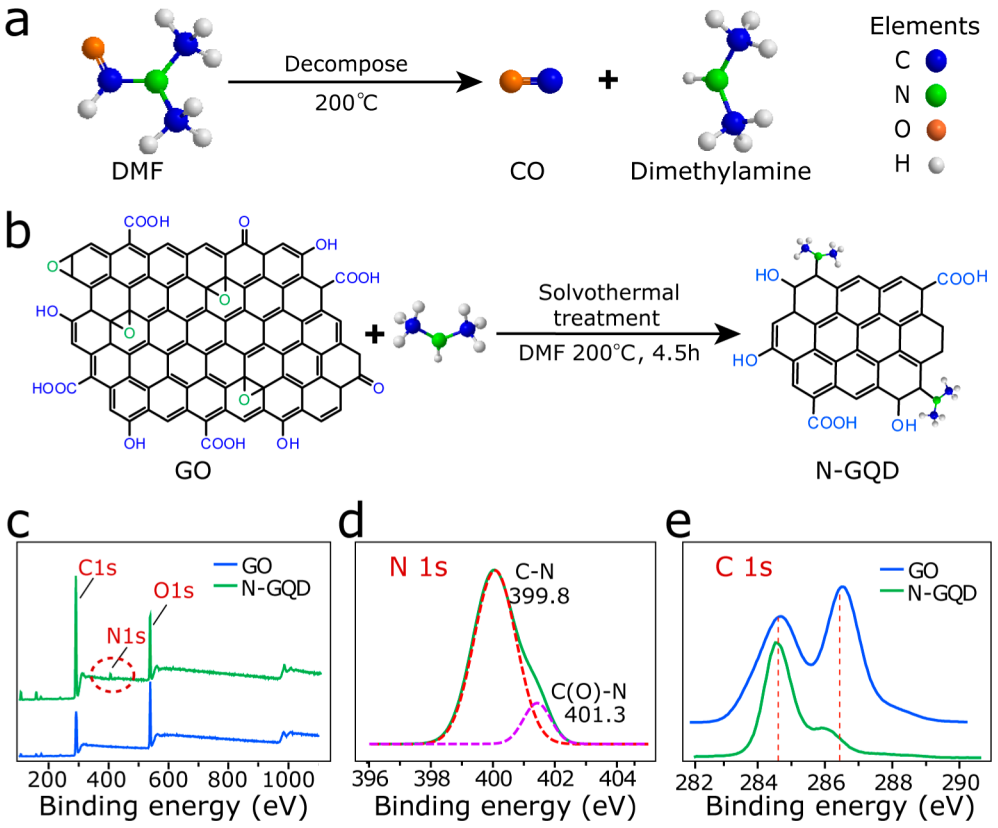

Figure 1. (a) Decomposition of DMF at a high temperature. (b) Schematic illustration of the strategy for the N-GQD preparation. (c) XPS survey spectra of GO and N-GQD. (d) High-resolution N 1s spectrum of N-GQD. (e) High-resolution C 1s XPS spectra of GO and N-GQD.

longer emission and excitation wavelengths,[25] which are less scattered by biotissues and more practical for bioimaging. Second, GQDs without passivation by any surfactant can exhibit strong fluorescence induced by a pronounced quantum confinement and edge effect,[14,26−28] which could also impart a larger two-photon absorption cross section and deeper penetration in turbid tissues.[29−31] Third, the large rigid π-conjugated electronic structure of GQD can also improve the intramolecular charge transfer efficiency and therefore enhance the two-photon absorption to achieve larger imaging depth in TPFI.[32]

To the best of our knowledge, no efforts have focused on the two-photon absorption and fluorescence property of GQD under femtosecond laser excitation, and no research about application of GQD as two-photon fluorescent probe for deep-tissue TPFI has been reported so far. In this work, we developed a facile solvothermal approach for doping nitrogen to GQD using dimethylformamide (DMF) as both solvent and nitrogen sources. Two-photon-induced fluorescence of N-GQD was systematically investigated using near-infrared (NIR) femtosecond laser as excitation and applied for efficient two-photon cellular and deep-tissue imaging. The large imaging depth achieved by N-GQD significantly extends the fundamental two-photon imaging depth limit in scattering tissues. Furthermore, the good biocompatibility and extraordinary photostability support the potential application of N-GQD in long-term TPFI of biological tissues.

The N-GQD was prepared through a facile one-pot solvothermal approach using GO as a precursor. GO was obtained by a modified Hummer's method.[33] This chemically derived GO is a two-dimensional network of sp^2- and sp^3-bonded atoms and shows unique heterogeneous chemical structure in which aromatic sp^2 domains are surrounded by sp^3-hybridized carbon atoms. The sp^2 domains in GO are calculated to have a mean size of 2.7 nm according to the empirical Tuinstra−Koenig relationship.[25,34] To effectively introduce nitrogen with strong electron-denoting effect into GQD, DMF served as a solvent and source of nitrogen as it could be decomposed to dimethylamine[35] (a strong electron denoting group) and carbon monoxide at temperature higher than its boiling point (Figure 1a). Then the decomposed dimethylamine was doped into the GO to yield 1,2-amino alcohol via nucleophilic ring-opening reaction with the epoxy group on the surface of GO,[25,36] thus enabling the extraction of smaller sp^2 domains from the large GO sheet and simultaneous bonding of dimethylamine with the aromatic ring to form N-GQD as illustrated in Figure 1b. The XPS survey spectrum of N-GQD shows a pronounced N 1s peak with the N/C atomic ratio of 2.28%, while no N signal can be observed for the GO (Figure 1c). As the N-GQD sample for XPS characterization has been purified by dialyzing for several days to remove all of the DMF residues in N-GQD sample, it is safe to conclude that observed N 1s peak in Figure 1c is attributed to the solvothermal doping of GQD with N (see detailed information about the N-GQD purification in the Supporting Information). The high resolution XPS spectrum of N 1s from N-GQD (Figure 1d, solid line) can be deconvoluted into two peaks (dashed lines). The main peak at 399.8 eV is attributed to the N 1s of the N−C bond of amino alcohols, indicating that the decomposed dimethylamine is attached to the aromatic ring of the N-GQD. The minor peak at 401.3 eV is ascribed to the N−C bond of amide linkage, which is not shown in the schematic

dx.doi.org/10.1021/nl400368v | *Nano Lett.* 2013, 13, 2436−2441

due to its extremely low content in the N-GQD.[36] Furthermore, the C 1s spectrum of N-GQD (Figure 1e) shows the intensity of the peak at high binding energy (oxide carbon) obviously decreases while the peak at 284.8 eV (sp^2 bonded carbon) turns stronger compared with that of GO, disclosing the reduction of GO and the restoration of π-conjugated network.[37,38] A detailed analysis of C 1s spectra after the deconvolution treatment (Figure S2 in the Supporting Information) and the FT-IR spectra (Figure S3) of GO and N-GQD further suggests the reduction and nitrogen-doping mainly occur on the basal plane of GO by removing the epoxy groups and introducing the dimethylamido. These changes of chemical composition from GO to N-GQD is because that the epoxy group on the surface is more active than the carboxyl at the edge to react with the decomposed dimethylamine through a ring-opening amination to yield 1,2-amino alcohol during the solvothermal process.

A transmission electron microscopy (TEM) image (Figure 2a) shows the uniformly dispersed N-GQDs with an average

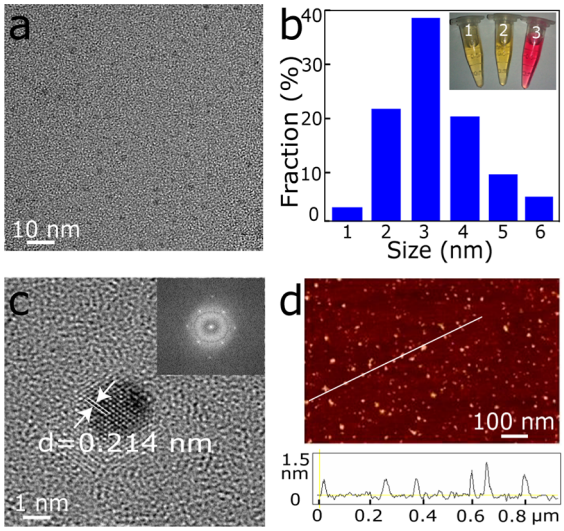

Figure 2. (a) TEM image of N-GQDs. (b) Diameter distribution of N-GQDs, and inset is the N-GQD dissolved in water (1), PBS (2), and DMEM high glucose culture medium with serum (3). (c) HRTEM image of N-GQD, and inset is the FFT pattern. (d) AFM image of N-GQDs deposited on the mica substrate and the height profile along the white line in the AFM image.

diameter of 3 nm (Figure 2b). The obtained N-GQD solution has a high zeta potential (−21 mW in water) and is very stable, exhibiting a transparent homogeneous phase without any precipitation or agglomeration at room temperature for at least 20 months either in water or physiological conditions such as phosphate buffer solution (PBS) and DMEM high glucose culture medium with serum (inset of Figure 2b). A well-resolved crystal lattice in the high resolution TEM (HRTEM) image (Figure 2c) gives evidence for the crystalline structure of the N-GQD. The lattice fringes of an N-GQD with a d spacing of 0.214 nm fit well with the (100) facet of graphene.[15] The corresponding fast Fourier transform (FFT) pattern (inset of Figure 2c) shows the hexagonal carbon network of N-GQD. The AFM image (Figure 2d) indicates the heights of the N-GQDs are between 0.5 and 1 nm, suggesting most of the N-GQDs are monolayer quasi-round graphene nanosheets.

UV−vis spectrum of N-GQD aqueous solution in Figure 3a shows an absorption band at ca. 230 nm, which is ascribed to

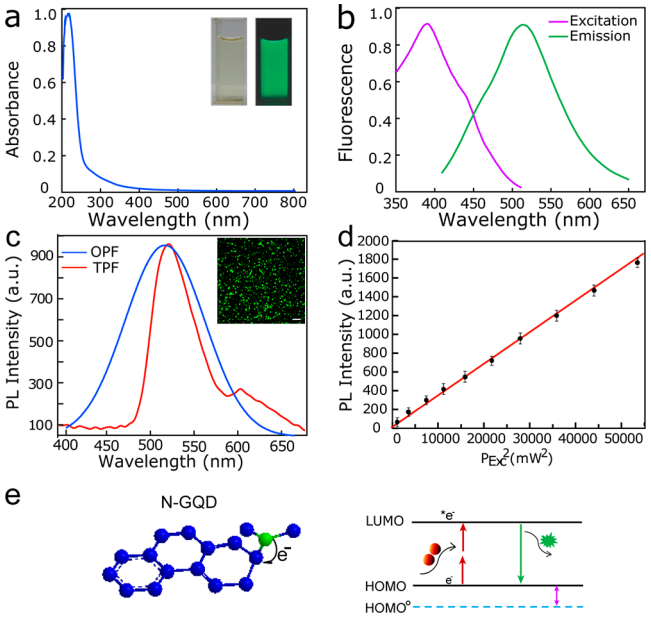

Figure 3. (a) UV−vis absorption spectrum of N-GQD aqueous solution. Inset: Photograph taken without (right) and with (left) UV lamp irradiation (365 nm). (b) One-photon fluorescence excitation (purple line) and emission (green line) spectra of N-GQD aqueous solution. (c) Two-photon-induced fluorescence spectrum of N-GQD solution under 800 nm femtosecond laser excitation. Inset: Two-photon fluorescence image of solid N-GQD (scale bar: 10 μm). (d) Quadratic relationship of the fluorescence intensity of the N-GQD aqueous solution with the different excitation laser powers at 800 nm (P_{Exc}, as measured at the focal plane). (e) Fluorescence mechanism of N-GQD.

the $\pi-\pi^*$ transition of C═C. The optical absorption edge is found to be 390 nm, revealing a 3.2 eV optical bandgap of N-GQD. Under irradiation with a 365 nm UV lamp, the N-GQD emits strong green fluorescence as shown in the inset of Figure 3a. The one-photon fluorescence excitation and emission spectra in Figure 3b shows the maximum excitation and emission wavelength are located at 390 and 520 nm, respectively. The lifetime of the fluorescence was determined to be 6.27 ns (Figure S4), similar to that of the organic molecules. From this point of view, the ultrasmall sized N-GQD can also be identified as an aromatic macromolecule.

The two-photon fluorescence of N-GQD was systemically investigated on a home-built optical setup. To directly excite the N-GQD samples with high photon density needed for two-photon absorption, an optical parametric oscillator (OPO, λ_{center} = 780 nm, 80 MHz repetition rate, 140 fs pulse width, OPAL BB, Spectra Physics) pumped by a mode-locked femtosecond Ti:Sapphire laser (Tsunami, Spectra Physics) was used as the excitation source. The generated two-photon fluorescence was recorded with a CCD camera (Newton, Andor) through a monochromator. Figure 3c shows the two-photon fluorescence spectrum of N-GQD solution under the excitation by the femtosecond pulse laser with a wavelength of 800 nm. For the obtained two-photon fluorescence spectrum, the maximum emission wavelength is indistinguishable with that of the one-photon fluorescence spectrum of N-GQD, but the bandwidth is much narrower than that of the one-photon fluorescence spectrum. The inset of Figure 3c is the two-photon fluorescence image of the dried N-GQD samples obtained on a two-photon microscope. To explore whether the

dx.doi.org/10.1021/nl400368v | Nano Lett. 2013, 13, 2436−2441

observed green fluorescence of N-GQD originates from two-photon absorption process with laser excitation in the NIR, the change of the green fluorescence intensity was monitored by adjusting the power of the 800 nm laser. As demonstrated in the Figure 3d, the obvious quadratic relationship between the fluorescence intensity and the excited laser power suggests the two-photon excitation is truly responsible for the green fluorescence in nature.[16]

For further evaluating the performance of the N-GQD for TPFI, the two-photon absorption cross section (σ_{2PA}) of N-GQD was measured using rhodamine B as a reference based on the equation, $\sigma_2 = \sigma_1 \times (F_2/F_1) \times (\phi_1/\phi_2) \times (C_1/C_2)$, where F represents the observed fluorescence intensity, ϕ stands for the quantum yield, C is the concentration, and the subscripts 1 and 2 denote the values for the N-GQD and rhodamine B, respectively.[39] The emission quantum yield (QY) of N-GQD aqueous solution was measured to be 0.31. Based on the above equation, a large σ_{2PA} of 48 000 GM with excitation at 800 nm achieves the highest value ever reported for carbon-based nanomaterials. This σ_{2PA} is 2 orders of magnitude larger than that of organic molecules and even comparable to that of the high-performance CdSe QDs.[40,41] The large σ_{2PA} is caused by the efficient intramolecular charge transfer, owing to the existence of large π-conjugated systems of N-GQD and the strong electron denoting effect of the doped dimethylamido. Meanwhile, the increased quantum confinement of the ultrasmall-sized N-GQD with highly symmetric bandgap can contribute to the high σ_{2PA} value.[29,31]

Similar to the chemical structure of polyaromatic compounds, the fluorescence may originate from the $\pi-\pi$ electron transition[17] since the N-GQD has large π-conjugated system and rigid plane as illustrated in Figure 3e. Furthermore, the lone pair electrons from the strong electron donating group dimethylamido which is doped to the aromatic ring of N-GQD, can be excited to the aromatic rings to form the p$-\pi$ conjugation, further enlarging the π-conjugated system.[39] The strong orbital interaction between dimethylamido and π-conjugated system of N-GQD elevates the primary HOMO° (blue dashed line) to a higher energy obit such as HOMO (black solid line), resulting in a decrease of bandgap and red-shift of fluorescence emission. More importantly, the large π-conjugated system in N-GQD and strong electron donating effect of dimethylamido can also facilitate the charge transfer efficiency,[36] enhancing the two-photon absorption and thus imparting strong two-photon-induced fluorescence for N-GQD.

To demonstrate the capability of the N-GQD for two-photon bioimaging, we carried out an in vitro bioimaging study using human cervical carcinoma Hela cells by a multiphoton fluorescence microscope. After incubation with the N-GQD (50 μg/1 mL DMEM high glucose) at 37 °C for 2 h, the Hela cells under living conditions became brightly illuminated when imaged under the microscope with excitation at 800 nm. The obtained images clearly visualize the bright field image of Hela cells (Figure 4a), high contrast fluorescence image of green N-GQDs distributed around each nucleus (Figure 4b), and the merged image of cell with the bright field and the green fluorescence images (Figure 4c), displaying that the N-GQD can label both the cell membrane and the cytoplasm of Hela cells without invading the nucleus in a significant fashion. To further confirm the location of N-GQD in cells, we also performed z-axis imaging of Hela cells (Figure S5 in the Supporting Information). As the z-axis moves from the top (0

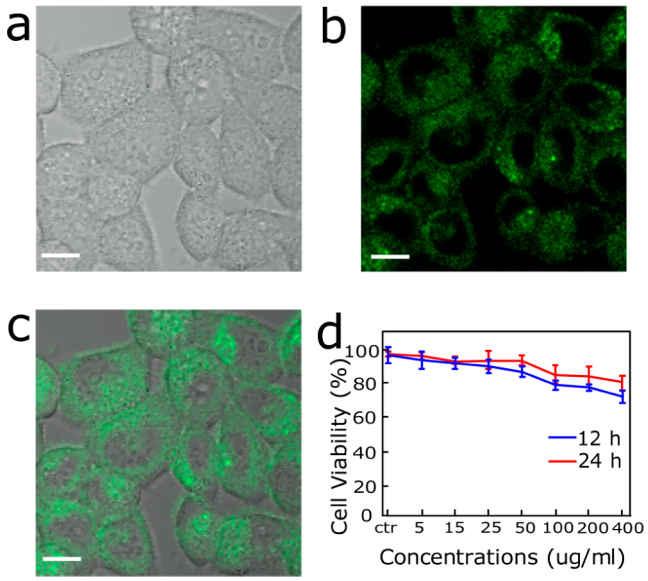

Figure 4. Two-photo cell imaging under (a) bright field and (b) 800 nm excitation. (c) The merged image of a and b. (All scale bars: 10 μm.) (d) Cell viability after incubation with N-GQD for 12 and 24 h.

μm) to the bottom (15 μm, Δz = 3 μm), we can clearly observe the fluorescence spots throughout the z axis of the Hela cells. Therefore, it is safe to state that N-GQDs have been uptaken by cells and locate inside the cytoplasm rather than bounded or adsorbed on the surface of Hela cells. It should be noted that a low laser power of 1 mW (average power density: 13 W cm^{-2}) was sufficient to induce strong fluorescence of the N-GQDs internalized in Hela cells (Figure 4b). Besides the strong two-photon fluorescence and good stability in the physiological conditions, the N-GQD also show quite low cytotoxicity as shown in Figure 4d. Different doses of N-GQDs (5−400 μg mL^{-1}) do not weaken the cell activity compared with the control group, as evaluated by the CCK-8 assay after coincubation of Hela cells with N-GQD for 12 and 24 h, respectively. The efficient cellular uptake, nontoxicity, and strong two-photon fluorescence show that N-GQD can be used as excellent two-photon probes for high contrast bioimaging.

For in vivo bioimaging applications, exact knowledge about the maximum tissue penetration depth of N-GQD is required. To explore the potential use of the strongly fluorescent N-GQD for deep tissue TPFI, we investigated the imaging depth of N-GQD in turbid tissue phantom for the first time. Intralipid was chosen as a mock tissue because of its similar scattering properties with the real tissues.[42] As shown in the schematic of our imaging setup (Figure 5a), a gap with adjustable height was created by putting double-sided adhesive with different layers between both ends of the two coverslips. Then a stock of Intralipid (20%) was diluted to make a 1% solution to fill up into the tunable gap of the two coverslips to simulate the biological tissues with different thickness. A drop of N-GQD aqueous solution was dripped on the top coverslip and then dried in the vacuum. And an inverted two-photon microscope with a 20× long working objective lens (0.45 NA) was used to image the N-GQDs at different depths in the mock tissue. The obtained two-photon fluorescence images (right panel of Figure 5b) demonstrate that the N-GQD can be imaged with high resolution and a high signal-to-noise ratio at depths ranging from 0 to 1300 μm in the tissue phantom using NIR laser as excitation source. Even at the depth of 1800 μm, we can easily

dx.doi.org/10.1021/nl400368v | Nano Lett. 2013, 13, 2436−2441

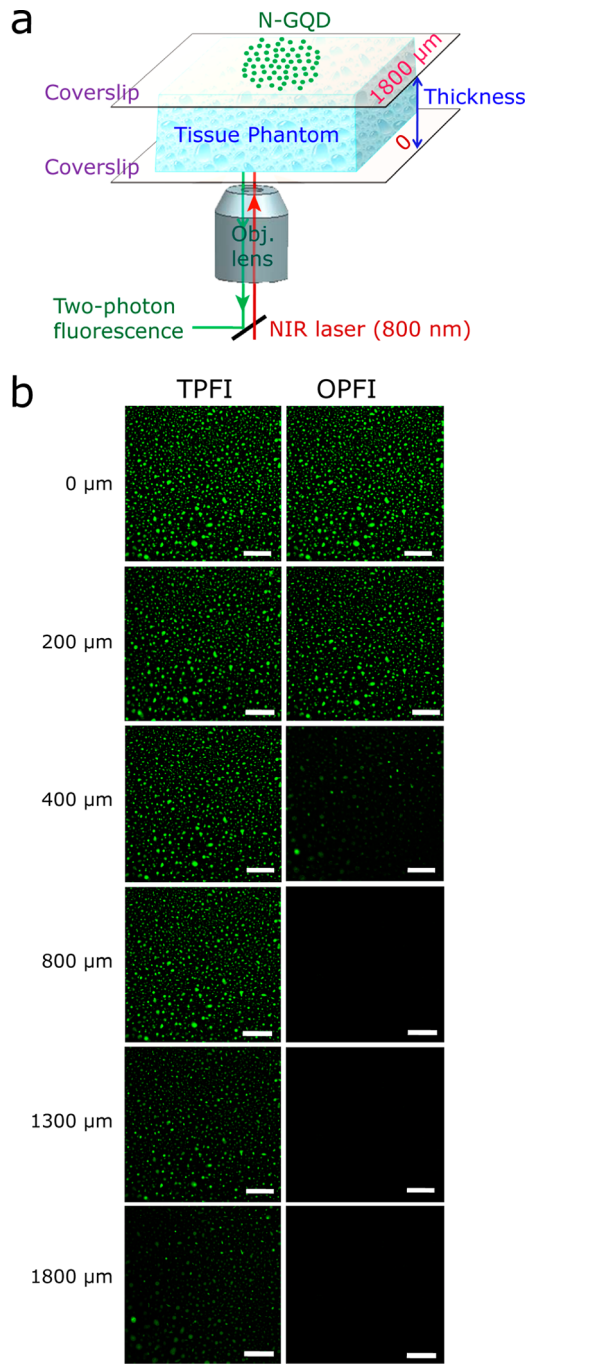

Figure 5. (a) Schematic of the setup used for TPFI of N-GQDs in tissue phantom with different thickness. (b) Penetration depth of N-GQDs for TPFI (right panel) and OPFI (left panel) in tissue phantom (all scale bar: 100 μm).

identify the N-GQDs in the tissue phantom with appreciable two-photon fluorescence signal, though the fluorescence intensity dramatically decreases. Besides, the monodispersed N-GQD solution sample can also emit a bright fluorescence signal even in deep tissue at 1800 μm (Figure S6 in the Supporting Information). In contrast, the OPFI (left panel of Figure 5b) shows that the maximum penetration depth is only 400 μm (even using the full output power for excitation) due to the strong scattering and refraction of the visible excitation light in turbid tissue phantom. The large two-photon imaging depth of 1800 μm achieved by the bright N-GQD is far exceeding that of the organic dyes and even larger than that of the semiconductor QDs.[43] The TPFI using N-GQD as fluorescent probe is particularly suitable for in vivo bioimaging applications where there is considerable interest in investigating bio-structures in the 800−1500 μm region.[44]

The excellent photostability of two-photon probes is also of great importance for TPFI, especially for the long-term dynamic bioimaging. Under continued laser excitation at 800 nm, the N-GQD exhibits no attenuation in fluorescence intensity, demonstrating their extraordinary photostability (Figure S7). Meanwhile, concerning the possible negative photothermal effect on living cells with NIR femtosecond laser excitation, we measured the temperature of the N-GQD aqueous solution upon irradiation with 800 nm femtosecond laser over different times. With continuous laser irradiation at the high power density, the temperature of the N-GQD aqueous solution showed little increase in temperature, similar to that of the pure water as shown in Figure S8. This negligible photothermal effect indicates that N-GQD could be applied for TPFI of living cells and tissues without causing any thermal damage to them. Moreover, the N-GQD was demonstrated to be strongly fluorescent in a wide pH range (Figure S9). The fluorescence emission of N-GQD is strongest in neutral or weakly alkaline conditions (pH = 7−9). Under acidic or strong alkaline conditions, the fluorescence intensity of N-GQD decreases by certain degrees. Even so, the N-GQD exhibits much stronger fluorescence than their N-free counterpart in the acid conditions (pH = 1−6), in which the fluorescence of the N-free GQD will be completely quenched.[14] This result suggests that the fluorescent N-GQD can be used in a wide pH range, such as tumor environment with a relatively low pH value.

Other types of graphene-based nanomaterials, such as graphene oxide nanoparticles (GON), have also been investigated for two-photon bioimaging. However, the mission QY of GON was reported too low to be measured, and a laser power of 7 mW was needed to induce photoluminescence of GONs in cells, while a low laser power of 1 mW was sufficient to excite strong two-photon fluorescence of N-GQD in cells in our work. More importantly, the two-photon absorption cross-section of N-GQD was measured to be as high as 48 000 GM and a large imaging depth of 1800 μm was achieved in tissue phantom using N-GQD as two-photon probes. But the two-photon absorption cross-section of GON was too low to calculate a specific value to compare with that of N-GQD and the maximum imaging depth of GON was much lower than that of N-GQD. The low efficiency of GON is because that the heavy oxidation of GON inhibits the electron−hole recombination and disrupts the intramolecular charge transfer, resulting in a low QY and small two-photon absorption cross-section. In contrast, the low O/C ratio of N-GQD reduces the inhibition the electron−hole recombination, obtaining a high QY. At the same time, the doped nitrogen with strong electron denoting effect enhances intramolecular charge transfer to achieve a large two-photon absorption cross-section for N-GQD. Besides, the N-GQD was much stable than GON under laser irradiation. No temperature increase was observed for N-GQD as shown in Figure S8. But for GON, the temperature increased dramatically upon irradiation with laser. For long-term bioimaging of living organism, the stable N-GQD is more suitable than GON as two-photon probes.

In conclusion, N-GQDs were facilely prepared by a one-pot solvothermal approach using DMF as solvent and nitrogen

dx.doi.org/10.1021/nl400368v | Nano Lett. 2013, 13, 2436−2441

source. The N-GQD exhibits a two-photon absorption cross section as high as 48 000 GM and are demonstrated as an efficient two-photon fluorescent probe for cellular and deep-tissue imaging. A large imaging penetration depth of 1800 μm achieved by N-GQD in tissue phantom significantly extends the fundamental imaging depth limit of two-photon microscopy. Furthermore, the N-GQD displays little photobleaching and photothermal effects under repeated femtosecond NIR laser irradiation and can emit quite strong fluorescence over a wide range of pH values. It is anticipated that the large imaging depth of N-GQD combining with their excellent biocompatibility and extraordinary photostability will impart potential use for advancing two-photon imaging in virtual applications such as monitoring the biological activity of deep tissues and noninvasively detecting disease of living biosystems.

■ ASSOCIATED CONTENT

Supporting Information

Experimental details for preparation of N-GQD, cellular imaging and cytotoxicity evaluation, measurement of absolute quantum yield, and supplementary results. This material is available free of charge via the Internet at http://pubs.acs.org.

■ AUTHOR INFORMATION

Corresponding Author

*E-mail: gongjr@nanoctr.cn.

Notes

The authors declare no competing financial interest.

■ ACKNOWLEDGMENTS

The authors acknowledge partial financial support for this work from the National Natural Science Foundation of China (Nos. 21005023, 91123003), the National Basic Research Program of China (No. 2011CB933401), and the Knowledge Innovation Program of the Chinese Academy of Sciences.

■ REFERENCES

(1) Denk, W.; Strickler, J. H.; Webb, W. W. *Science* **1990**, *248*, 73−76.
(2) Helmchen, F.; Denk, W. *Nat. Methods* **2005**, *2*, 932−940.
(3) Jung, W.; Tang, S.; McCormic, D. T.; Xie, T.; Ahn, Y. C.; Su, J. P.; Tomov, I. V.; Krasieva, T. B.; Tromberg, B. J.; Chen, Z. P. *Opt. Lett.* **2008**, *33*, 1324−1326.
(4) Fu, L.; Jain, A.; Cranfield, C.; Xie, H.; Gu, M. *J. Biomed. Opt.* **2007**, *12*, 40501−3.
(5) Theer, P.; Hasan, M. T.; Denk, W. *Opt. Lett.* **2003**, *28*, 1022−1024.
(6) Kobat, D.; Durst, M. E.; Nishimura, N.; Wong, A. W.; Schaffer, C. B.; Xu, C. *Opt. Express* **2009**, *17* (16), 13354−13364.
(7) Larson, D. R.; Zipfel, W. R.; Williams, R. M.; Clark, S. W.; Bruchez, M. P.; Wise, F. W.; Webb, W. W. *Science* **2003**, *300*, 1434−1436.
(8) He, G. S.; Tan, L. S.; Zheng, Q.; Prasad, P. N. *Chem. Rev.* **2008**, *108*, 1245−1330.
(9) Lee, J. H.; Lim, C. S.; Tian, Y. S.; Han, J. H.; Cho, B. R. *J. Am. Chem. Soc.* **2010**, *132*, 1216−1217.
(10) Zhu, M. Q.; Zhang, G. F.; Li, C.; Aldred, M. P.; Chang, E.; Drezek, R. A.; Li, A. D. Q. *J. Am. Chem. Soc.* **2010**, *133*, 365−372.
(11) Baker, S. N.; Baker, G. A. *Angew. Chem., Int. Ed.* **2010**, *49*, 6726−6744.
(12) Sun, X. M.; Liu, Z.; Welsher, K.; Robinson, J. T.; Goodwin, A.; Zaric, S.; Dai, H. J. *Nano Res.* **2008**, *1*, 203−212.
(13) Li, Q.; Ohulchanskyy, T. Y.; Liu, R.; Koynov, K.; Wu, D.; Best, A.; Kumar, R.; Bonoiu, A.; Prasad, P. N. *J. Phys. Chem. C* **2010**, *114*, 12062−12068.
(14) Pan, D. Y.; Zhang, J. C.; Li, Z.; Wu, M. H. *Adv. Mater.* **2010**, *22*, 734−738.
(15) Peng, J.; Gao, W.; Gupta, B. K.; Liu, Z.; Romero, R.; Ge, L. H.; Song, L.; Alemany, L. B.; Zhan, X. B.; Gao, G. H.; Vithayathil, S. A.; Kaipparettu, B. A.; Marti, A. A.; Hayashi, T.; Zhu, J. J.; Ajayan, P. M. *Nano Lett.* **2011**, *12*, 884−849.
(16) Cao, L.; Wang, X.; Meziani, M. J.; Lu, F.; Wang, H. F.; Luo, P. G.; Lin, Y.; Harruff, B. A.; Veca, L. M.; Murray, D.; Xie, S. Y.; Sun, Y. P. *J. Am. Chem. Soc.* **2007**, *129*, 11318−11319.
(17) Li, J. L.; Bao, H. C.; Hou, X. L.; Sun, L.; Wang, X. G.; Gu, M. *Angew. Chem., Int. Ed.* **2012**, *51*, 1830−1834.
(18) Qian, J.; Wang, D.; Cai, F. H.; Xi, W.; Peng, L.; Zhu, Z. F.; He, H.; Hu, M. L.; He, S. *Angew. Chem., Int. Ed.* **2012**, *51*, 10570−10575.
(19) Zhu, S.; Zhang, J.; Tang, S.; Qiao, C.; Wang, L.; Wang, H.; Liu, X.; Li, B.; Li, Y.; Yu, W.; Wang, X.; Sun, H.; Yang, B. *Adv. Funct. Mater.* **2012**, *22*, 4732−4740.
(20) Li, Y.; Zhao, Y.; Cheng, H. H.; Hu, Y.; Shi, G. Q.; Dai, L. M.; Qu, L. T. *J. Am. Chem. Soc.* **2012**, *134*, 15−18.
(21) Guo, B. D.; Liu, Q.; Chen, E. D.; Zhu, H. W.; Fang, L.; Gong, J. R. *Nano Lett.* **2010**, *10*, 4975−4980.
(22) Guo, B. D.; Fang, L.; Zhang, B. H.; Gong, J. R. *Electron. Lett.* **2011**, *47*, 663−664.
(23) Guo, B. D.; Fang, L.; Zhang, B. H.; Gong, J. R. *Insci. J.* **2011**, *1*, 80−89.
(24) Li, Q.; Zhang, S.; Dai, L.; Li, L. S. *J. Am. Chem. Soc.* **2012**, *134*, 18932−18935.
(25) Tetsuka, H.; Asahi, R.; Nagoya, A.; Okamoto, K.; Tajima, I.; Ohta, R.; Okamoto, A. *Adv. Mater.* **2012**, *24*, 5333−5338.
(26) Ponomarenko, L.; Schedin, F.; Katsnelson, M.; Yang, R.; Hill, E.; Novoselov, K.; Geim, A. *Science* **2008**, *320*, 356−358.
(27) Girit, Ç. Ö.; Meyer, J. C.; Erni, R.; Rossell, M. D.; Kisielowski, C.; Yang, L.; Park, C. H.; Crommie, M.; Cohen, M. L.; Louie, S. G. *Science* **2009**, *323*, 1705−1708.
(28) Loh, K. P.; Bao, Q. L.; Eda, G.; Chhowalla, M. *Nat. Chem.* **2010**, *2*, 1015−1024.
(29) Padilha, L. A.; Nootz, G.; Olszak, P. D.; Webster, S.; Hagan, D. J.; Van Stryland, E. W.; Levina, L.; Sukhovatkin, V.; Brzozowski, L.; Sargent, E. H. *Nano Lett.* **2011**, *11*, 1227−1231.
(30) Luo, Z. T.; Vora, P. M.; Mele, E. J.; Johnson, A. T. C.; Kikkawa, J. M. *Appl. Phys. Lett.* **2009**, *94*, 111909−3.
(31) Trauzettel, B.; Bulaev, D. V.; Loss, D.; Burkard, G. *Nat. Phys.* **2007**, *3*, 192−196.
(32) Collini, E. *Phys. Chem. Chem. Phys.* **2012**, *14*, 3725−3736.
(33) Xu, Y.; Bai, H.; Lu, G.; Li, C.; Shi, G. *J. Am. Chem. Soc.* **2008**, *130*, 5856−5857.
(34) Tuinstra, F.; Koenig, J. L. *J. Chem. Phys.* **1970**, *53*, 1126−1130.
(35) Ai, K. L.; Liu, Y. L.; Lu, L. H.; Cheng, X. L.; Huo, L. H. *J. Mater. Chem.* **2011**, *21*, 3365−3370.
(36) Mei, Q. S.; Zhang, K.; Guan, G. J.; Liu, B. H.; Wang, S. H.; Zhang, Z. P. *Chem. Commun.* **2010**, *46*, 7319−7321.
(37) Compton, O. C.; Dikin, D. A.; Putz, K. W.; Brinson, L. C.; Nguyen, S. T. *Adv. Mater.* **2010**, *22*, 892−896.
(38) Li, Q.; Guo, B. D.; Yu, J. G.; Ran, J. R.; Zhang, B. H.; Yan, H. J.; Gong, J. R. *J. Am. Chem. Soc.* **2011**, *133*, 10878−10884.
(39) Xu, C.; Webb, W. W. *J. Opt. Soc. Am. B* **1996**, *13*, 481−491.
(40) Zipfel, W. R.; Williams, R. M.; Webb, W. W. *Nat. Biotechnol.* **2003**, *21*, 1369−1377.
(41) Pu, S. C.; Yang, M. J.; Hsu, C. C.; Lai, C. W.; Hsieh, C. C.; Lin, S. H.; Cheng, Y. M.; Chou, P. T. *Small* **2006**, *2*, 1308−1313.
(42) Welsher1, K.; Sherlock, S. P.; Dai, H. J. *Proc. Natl. Acad. Sci. U.S.A.* **2011**, *108*, 8943−8948.
(43) Maestro, L. M.; Ramírez-Hernández, J. E.; Bogdan, N.; Capobianco, J. N.; Vetrone, F.; Solé, J. G.; Jaque, D. *Nanoscale* **2012**, *4*, 298−302.
(44) Masters, B. R.; So, P. *Handbook of biomedical nonlinear optical microscopy*; Oxford University Press: New York, 2008.

Supporting Information

Strong Two-Photon-Induced Fluorescence from Photostable, Biocompatible Nitrogen-Doped Graphene Quantum Dots for Cellular and Deep-Tissue Imaging

Qian Liu, Beidou Guo, Ziyu Rao, Baohong Zhang, Jian Ru Gong*

National Center for Nanoscience and Technology, 11 Zhongguancun Beiyitiao, Beijing 100190, China
E-mail: gongjr@nanoctr.cn

http://www.nanoctr.cn/gongjianru

I. Experimental Section

1. N-GQD Preparation

The N-GQD was prepared through a facile one-pot solvothermal method. In brief, the graphene oxide (GO) was dissolved in dimethylformamide (DMF) with a concentration of ~200 mg ml^{-1}. The GO and DMF mixed solution was ultrasonicated for 30 minutes (120 W, 100 kHz) and then transferred to a poly(tetrafluoroethylene)-lined autoclave (30 ml) and heated at 200℃ for 4.5 h. After cooling to room temperature naturally, the obtained mixture was filtered through a 0.22 μm microporous membrane to remove the black precipitates, obtaining a brown solution. The solvent was removed with the aid of a rotary evaporator. Then the obtained N-GQD was dispersed in DI water. In fact, heating DMF at 200 ℃ for 4.5 h generated a small amount of impurities which could not be totally removed by evaporation. We further found that these DMF residues could emit blue fluorescence under UV lamp irradiation. Therefore, the obtained N-GQD must be dialyzed through a 500 Da dialyzer for at least 48 hours to totally remove the DMF residues until there was no blue fluorescence detected in the dialysis solution outside the dialyzer bag. Then the obtained pure N-GQD was used for further characterization.

The control experiment was also performed in the absence of DMF. GO was dissolved in DI water and applied for hydrothermal process under the same conditions. Under UV irradiation, the obtained GQD without nitrogen doping showed blue fluorescence rather than the green fluorescence of N-GQD. The fluorescence spectrum of GQD aqueous solution showed a maximum fluorescence peak at 450 nm (Ex 390 nm), which was consistent with the reported papers. Compared with GQD, the maximum emission peak shifted to 520 nm for N-GQD (Figure S1) with the same excitation wavelength, indicating the solvothermal process using DMF could successfully realize the nitrogen doping of GO to form the new N-GQD.

2. Characterization

Transmission electron microscopy (TEM) images and high-resolution transmission electron microscopy (HRTEM) images were collected on an F20 S-TWIN electron microscope (Tecnai G2, FEI Company), using a 200 kV accelerating voltage. Atomic force microscopy (AFM) images were obtained by a Dimension 3100 AFM, operating in tapping mode with a scan rate of 1.20 Hz and a resolution of 512×512 pixels. A nitrogen-doped silicon tip with 1-10 Ω cm phosphorus (Veeco, MPP-11100-140) was used as the probe. X-ray photoelectron spectroscopy (XPS) data were obtained by an ESCALab220i-XL electron spectrometer from VG Scientific using 300 W Al Kα radiation. The base pressure was about 3×10^{-9} mbar. The binding energies were referenced to the C 1s line at 284.8 eV from adventitious carbon. Curve fitting of the C 1s and N 1s spectra was performed using a Gaussian-Lorentzian peak shape. FT-IR spectra of the samples were recorded on IRAffinity-1 FTIR spectrometer. One-photon fluorescence spectra was measured on a Fluorolog3-21-iH320 spectrofluorometer (Jobin Yvon, France). All spectra were recorded with quartz cells of 10 mm path length.

3. Emission Quantum Yield (QY) Measurement of N-GQD.

The emission QY of N-GQD aqueous solution was measured on a Fluorolog3-21-iH320 spectrofluorometer (Jobin Yvon, France) equipped with an integrating sphere. The PLQY is determined using a method based upon that originally developed by de Mello et al.[2] In this approach, the value of the QY is calculated according to:[1]

$$\phi_{\mathrm{PL}} = \frac{E_{\mathrm{in}}(\lambda) - (1-\alpha)E_{\mathrm{out}}(\lambda)}{X_{\mathrm{empty}}(\lambda)\alpha},$$

with

$$\alpha = \frac{X_{\text{out}}(\lambda) - X_{\text{in}}(\lambda)}{X_{\text{out}}(\lambda)}$$

In these equations, $E_{\text{in}}(\lambda)$ and $E_{\text{out}}(\lambda)$ are the integrated luminescence as a result of direct excitation of the film (sample IN) and secondary excitation (sample OUT), respectively. $X_{\text{empty}}(\lambda)$ is the integrated excitation profile with the empty sphere. $X_{\text{in}}(\lambda)$ is the integrated excitation when the sample lies directly in the excitation path and $X_{\text{out}}(\lambda)$ is the integrated excitation when the excitation light first hits the sphere wall as previously explained.

4. Two-Photon Cellular Imaging.

A Nikon Fluoview multiphoton microscope (FV1000MPE) was used for two-photon luminescence imaging of N-GQD and Hela cells. A mode-locked Ti:Sapphire laser (MaiTai, Spectra Physics) with pulses of 100 fs at a repetition rate of 80 MHz was used as the excited light source. For cellular imaging, Hela cells were cultured in high-glucose modified Eagle's medium supplemented with 10% fetal bovine serum and 1% penicillin/streptomycin (HDMEM) using a four-chambered Lab-Tek coverglass system (Nalge Nunc) (approximately 5×10^5 in each well). All cells were incubated at 37 ℃ in a CO_2 incubator until approximately 80% confluence was reached. The aqueous solution of the N-GQD (1 mg ml^{-1}) was filtered through a 0.22 μm membrane (Millipore Express). Then the filtered solution (~50 μl) was mixed with the culture medium (1,000 μl) and added to three wells of the glass slide chamber (the fourth well used as a control) in which the Hela cells were grown. After incubation for 2 h, the Hela cells were washed three times with PBS (500 μl each time) and kept in PBS for two-photon imaging on the FV1000MPE with excitation at 800 nm using a water objective lens (60×). The laser power used for two-photon imaging was measured to be 1mW at the focal plane.

5. Cytotoxicity Evaluation.

The cells were cultured first for 24 h in an incubator (37 ℃, 5% CO_2), and for another 24 h after the culture medium was replaced by DMEM high glucose containing the N-GQD at different concentrations (0, 5, 15, 25, 50, 100, 200, 400 μg ml^{-1}). Then, 10 μl CCK-8 reagents mixed with 100 μl DMEM high glucose was added to each cell well. After further incubation for 4 h, the optical density (OD) of the mixture was measured at 450 nm. The cell viability was estimated according to the following equation: Cell Viability [%] = (OD_{treated} / OD_{control}) × 100%

($OD_{control}$ was obtained in the absence of N-GQD, and $OD_{treated}$ obtained in the presence of N-GQD.) Each experiment was performed four times and the average data was presented.

6. Two-Photon Deep-Tissue Imaging.

For the 0~800 μm imaging depth, the excitation powers were adjusted so that approximately the same signal-to-noise ratio (SNR) could be achieved at a constant frame rate of 1 fps, starting with 20 mW for the 0 um imaging depth. At the imaging depths beyond 800 μm, the full output power corresponding to approximately 100 mW average power of the OPO was used to achieve the fluorescence image of N-GQD in the turbid tissue phantom with a quite high SNR.

II. Supplementary Results and Discussion

1. Fluorescence Spectra of GQD and N-GQD

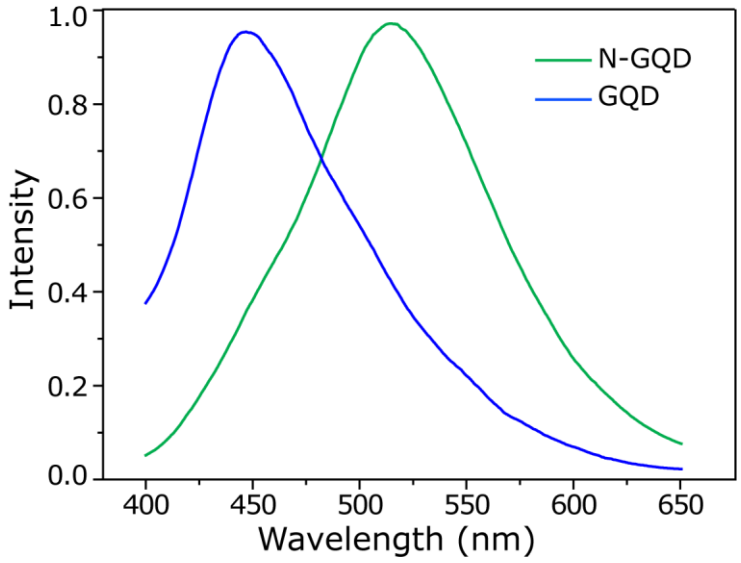

Figure S1. Fluorescence spectra of GOD (blue line) and N-GQD(green line), Ex: 390 nm.

2. High-Resolution C1s Spectra of GO and N-GQD

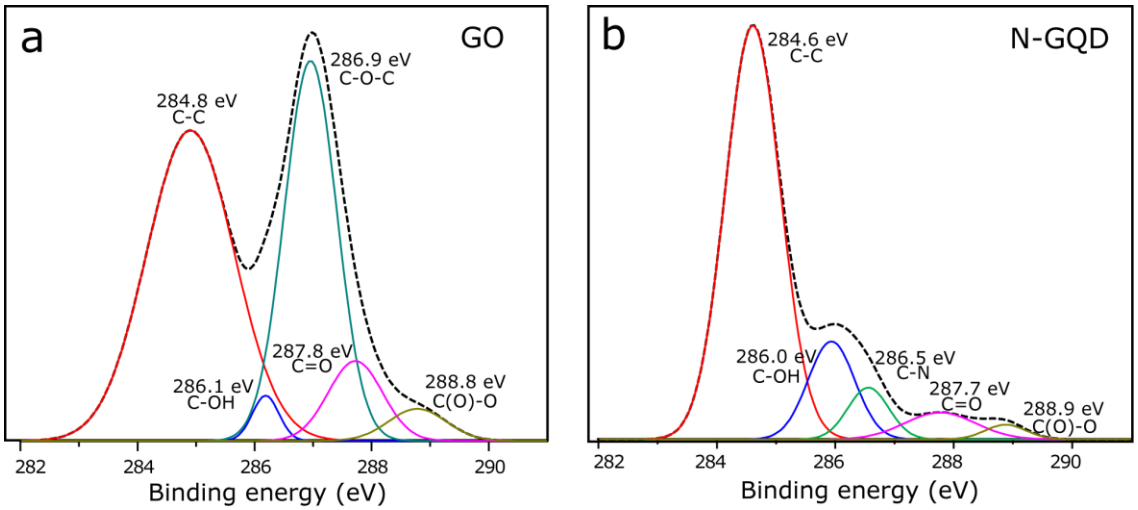

Figure S2. Deconvolution treatment of the C1s spectra of GO (a) and N-GQD (b).

The comparison of C1s (Figure S2) demonstrates the obvious change in carbon chemical environment from GO to N-GQD. The result of deconvolution treatment for the C 1s spectrum (Figure S2, a) of GO reveals four peaks at 284.8 (C-C, sp^2 bonded carbon), 286.1 (C-OH, hydroxyls), 286.9 (C-O-C, epoxy), 287.8 (C=O, carbonyls), and 288.8 eV (C(O)-O, carboxyl),[2,3] indicating the high percentage of oxygen-containing functional groups. In comparison, for the C1s spectrum of N-GQD (Figure S2, b), a new peak is presented at 285.9 eV, which is attributed to the C bound to the nitrogen, consistent well with the high N1s spectrum, revealing the doping of N atoms in N-GQD. At the same time, the peak of epoxy (286.9 eV) vanishes, while the peaks of hydroxyl (286.0 eV), carbonyl (287.7 eV) and carboxyl (288.9 eV) still exist, indicating the elimination of epoxy on the surface and the retention of hydroxyl, carbonyl, and carboxyl at the edge of N-GQD during the solvothermal process. Furthermore, the O/C atomic ratio for the N-GQD is 18%, which is lower than that of the GO (35%), indicating the reduction of GO. It is noted that the reduction mainly happens on the surface of N-GQD by removing the active epoxy, while most hydroxyl and carboxyl at the edge still exist.

3. FT-IR Spectra of GO and N-GQD

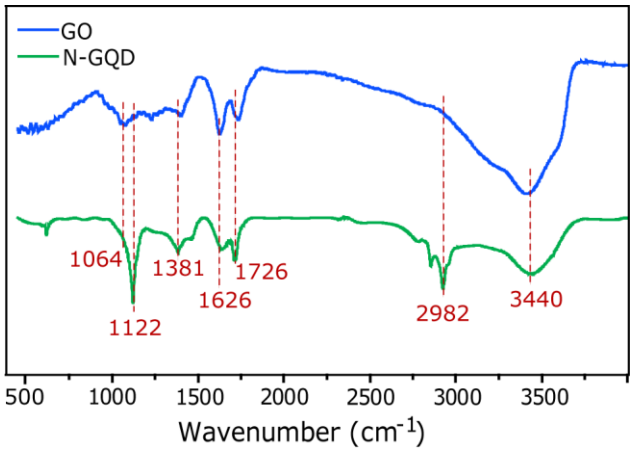

Figure S3. FT-IR spectra of GO and N-GQD

FT-IR spectra of GO and N-GQD (Figure S3) also confirms the nitrogen doping and partial reduction for N-GQD. Compared with the spectrum of GO, the epoxy band at 1064 cm^{-1} completely disappears while two new bands at 1123 and 2982 cm^{-1}, which are respectively assigned to the C-N-C asymmetric stretching and the C-H asymmetric stretching for the attached dimethylamido, can be observed for the spectrum of N-GQD.[2,4] And the bands at 1381 (bending vibration of O-H), 1626 (stretching vibrations C=C), 1713 (stretching vibrations of C=O in carbonyl groups), and 3440 cm^{-1} (stretching vibrations of O-H in hydroxyl) are present for both GO and N-GQD. Consistent well with the XPS data (in the text), these results suggest the elimination of epoxy groups and the chemical bonding of nitrogen groups on the basal C-C plane, whereas most of the inactive carboxyl and hydroxyl groups are still retained at the edge of the N-GQD.

4. Fluorescence Lifetime of N-GQD

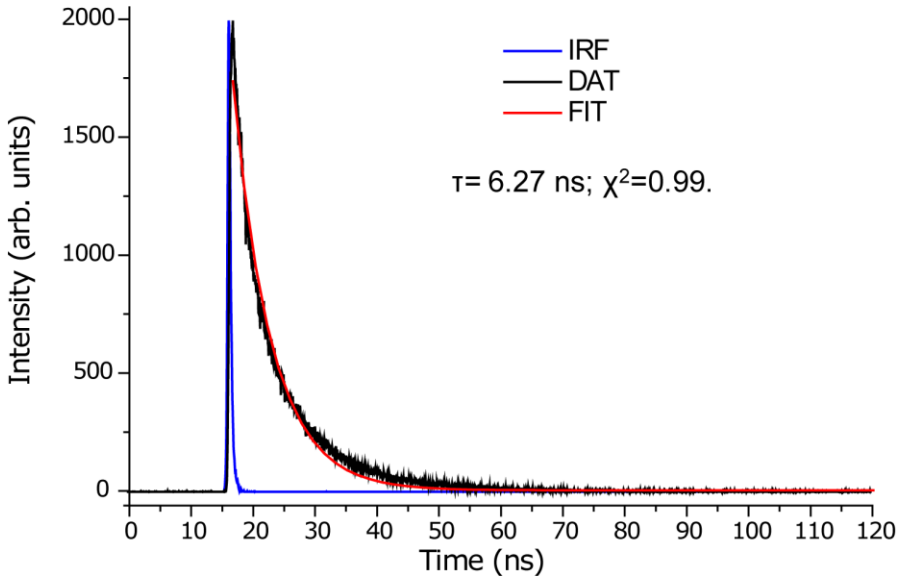

Figure S4. Fluorescence decay of N-GQD (Ex: 390 nm, Em: 520 nm)

The fluorescence lifetime of 6.27 ns indicates that the fluorescence process of N-GQD is similar to that of the organic molecules. And the rapid rates of recombination measured here provide strong evidence that the observed emission may result from dipole-allowed recombination across the direct bandgap transition in N-GQD. The observed fluorescence lifetime of N-GQD in nanosecond scale suggests that it is suitable for biological imaging and optoelectronic applications.

5. Two-Photon Fluorescent Images of Cells at Different Z Positions

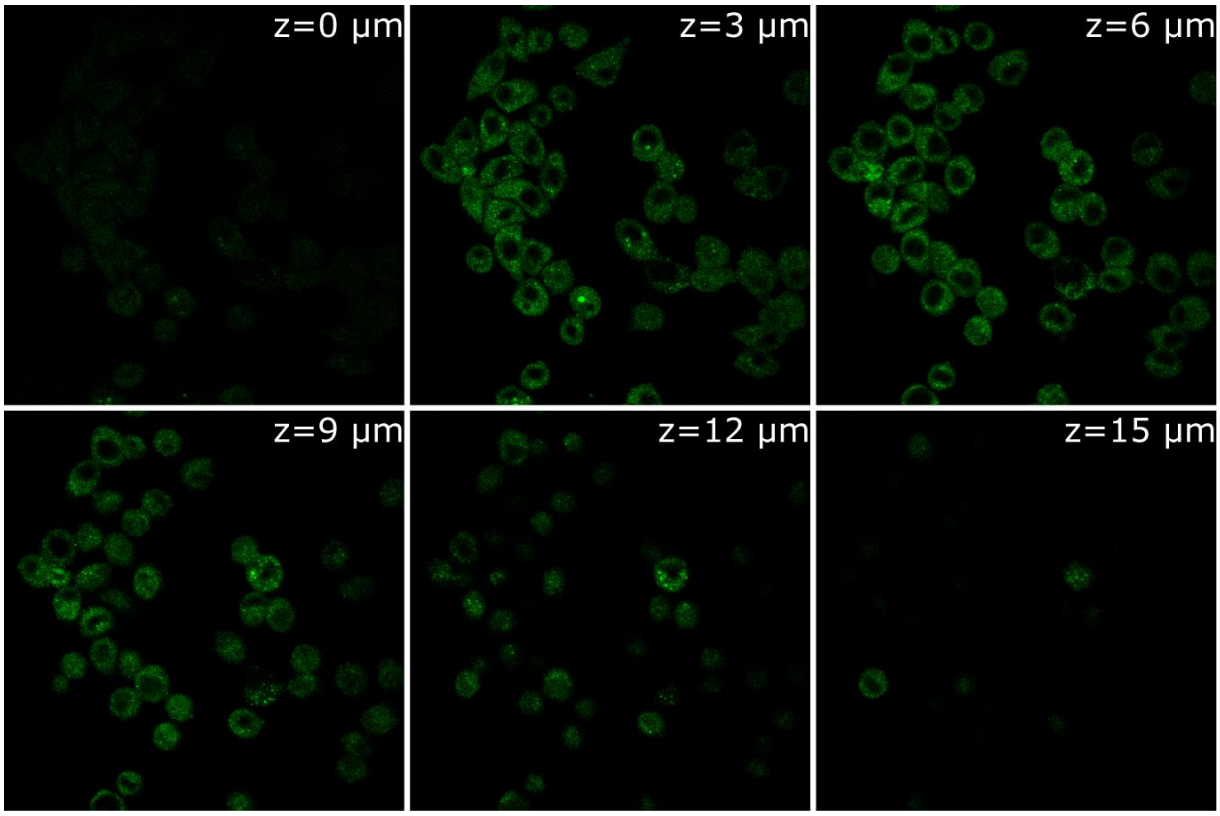

Figure S5. Fluorescent images of cells incubated with N-GQDs at different Z positions (from the top 0 μm to the bottom 15 μm, Δz = 3 μm)

As the z axis moves from the top (0 μm) to the bottom (15 μm, Δz = 3μm), we can clearly observe the fluorescence spots throughout the z axis of the Hela cells. Therefore, it is safe to state that N-GQDs have been uptaken by cells and locate inside the cytoplasm rather than bounded or adsorbed on the surface of Hela cells.

6. Deep-Tissue Imaging Using the Monodispersed N-GQD Aqueous Solution

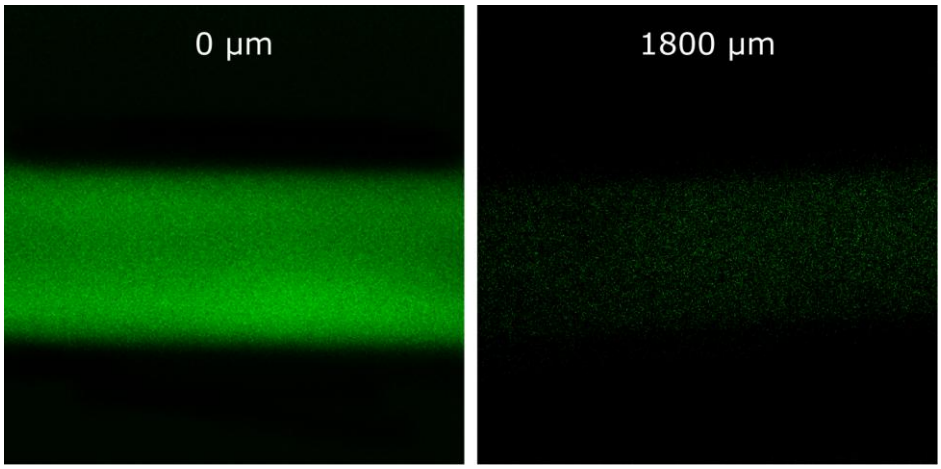

Figure S6. Deep-tissue imaging using the monodispersed N-GQD solution loaded in a capillary

Deep-tissue imaging using the monodispersed N-GQD solution sample was also performed. We carefully used a capillary to load N-GQD aqueous solution. Then the capillary filled with N-GQD solution was placed in the tissue phantom for two-photon imaging. As shown in Figure S6 in the Supporting Information, the N-GQD solution sample could also emit bright fluorescence signal even in the deep tissue (~1800 μm). And the large two-photon absorption cross section and the high fluorescence QY could contribute to the bright fluorescence signal observed in the deep tissue. However, the focal plane was difficult to control at the same place of the capillary when we had to constantly adjust the capillary to locate at the different depth of the tissue phantom during the imaging experiment. So we used the dried N-GQD samples deposited on a coverslip which was marked with a red spot to help focusing on the same place of the coverslip at different imaging depths.

7. Photostability of N-GQD under NIR Laser Irradiation and UV Irradiation

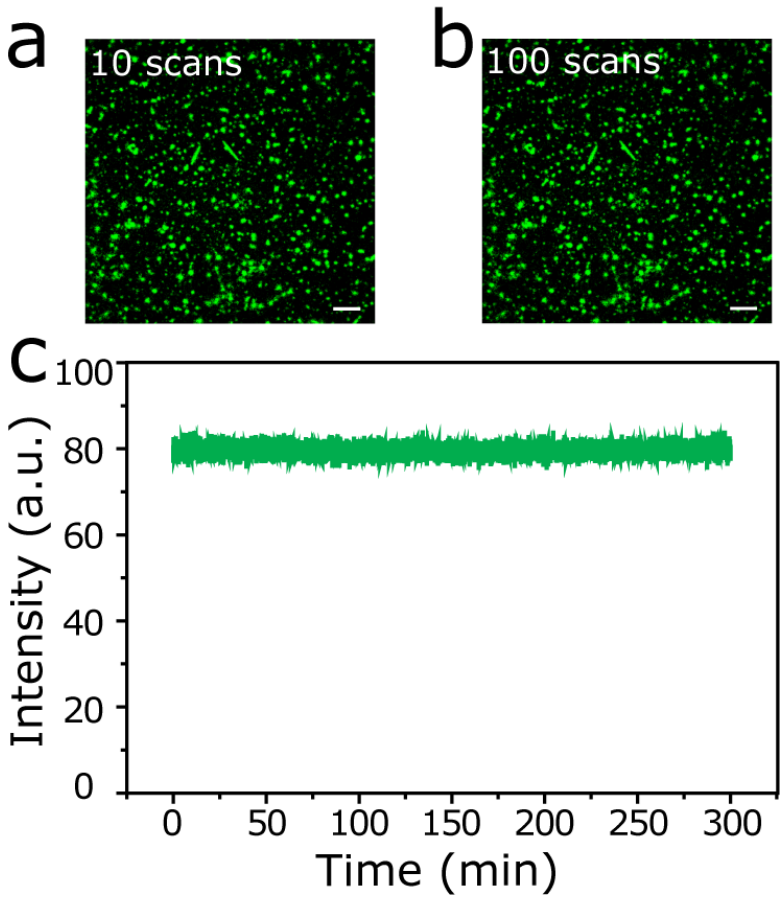

Figure S7. (a, b) Photostability of N-GQD under NIR laser irradiation; (c) Time-dependent fluorescence behavior of N-GQD under UV irradiation.

The N-GQD was found to be extraordinarily photostable, showing no meaningful changes in the fluorescence intensity (Figure S7 a,b) after being scanned for one hundred times under laser excitation at 800 nm. The photostability of the N-GQD was also demonstrated by recording the fluorescence intensity with continuous UV irradiation using the Xe light (390 nm, 300 mW). After continuous irradiation for 5 h as shown in Figure S7, the emission intensity collected at 530 nm didn't show any decrease.

8. Photothermal Effect of N-GQD under NIR Femtosecond Laser Irradiation

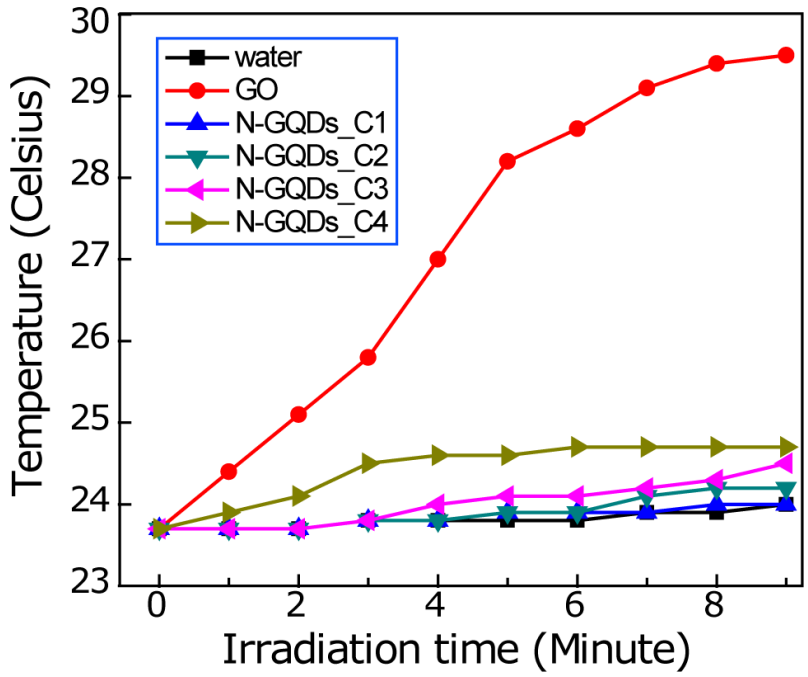

Figure S8. Photothermal effect of GO and N-GQD under NIR laser irradiation

To be on the safe side, we measured the temperatures of N-GQD aqueous solution upon irradiated with 800 nm femtosecond laser at power density of 3 W cm^{-2} over different times. Interestingly, under continuous laser irradiation with high power density, the temperature of the N-GQD aqueous solution showed little change in temperature, similar to the pure water (—■—) as shown in Figure S8. Nearly no heating effect is observed for the N-GQD solution with different concentrations (—▲—0.05 mg ml^{-1}, —▼—0.2 mg ml^{-1}, —◀—1 mg ml^{-1}, 0.05 mg ml^{-1} is already much higher than the concentration required for imaging) under fs pulse laser irradiation for even 9 minutes. Even for the N-GQD with a concentration as high as —▶—5 mg ml^{-1}, the temperature of N-GQD aqueous solution totally increased less than 1 centigrade after irradiation for 9 minutes. In contrast, the GO aqueous solution with a low concentration (—●—1 mg ml^{-1}) increased almost 10 degrees centigrade. In fact, this serious heating effect under irradiation can cause damage even destruction to the health cells and tissues. From the safe points of view, comparing with GO, the photothermal stable N-GQD is much more suitable for long-term imaging of living biological tissues, especially in two-photon bioimaging using a high power laser as excitation source.

9. pH-Dependent Fluorescence Emission of N-GQD

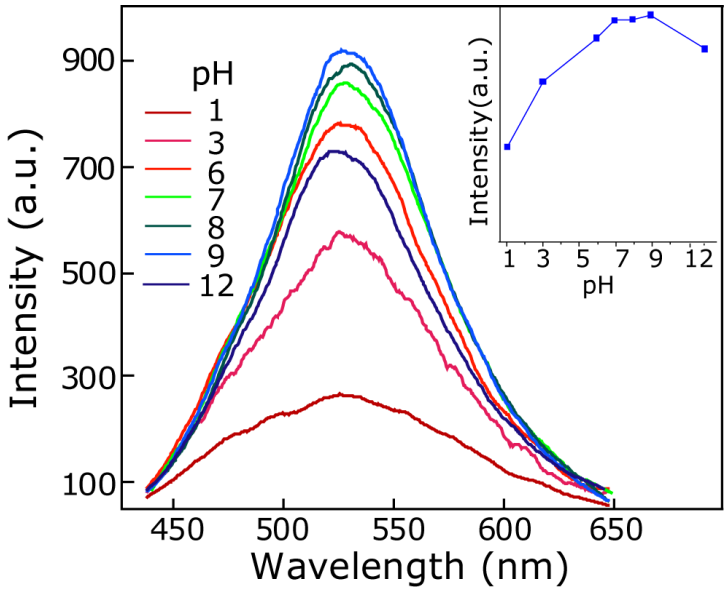

Figure S9. pH-dependent fluorescence emission of N-GQD (Ex: 365 nm)

Influence of the chemical environment on fluorescence behavior of N-GQD was investigated at pH values varying from 1 to 12 (Figure S9). The pH dependent PL emission is summarized in the inset of Figure S9. Under neutral or weakly alkaline conditions (pH = 7~9), the N-GQD emits the strongest fluorescence at 530 nm. Under acidic or strong alkaline conditions, the emission intensity of N-GQD decreases by certain degree. Even so, the N-GQD exhibits much stronger fluorescence than their N-free counterpart in the acid conditions (pH = 1~6), in which the fluorescence of the N-free GQD will be completely quenched. These results suggest that the luminescent N-GQD can be used in a wide pH range, such as tumor cell with a relatively low pH value.

References

(1) Porres, L.; Holland, A.; Pålsson, L.O.; Monkman, A. P.; Kemp, C.; Beeby, A. *J. Fluoresc.* **2006**, *16*, 267.

(2) Compton, O. C.; Dikin, D. A.; Putz, K. W.; Brinson,L. C.; Nguyen, S. T. *Adv. Mater.* **2010**, *22*, 892.

(3) Li, Q.; Guo, B.; Yu, J.; Ran, J.; Zhang, B.; Yan, H. J.; Gong, J. R. *J. Am. Chem. Soc*. **2011**. *133*, 10878.

(4) Mei, Q.; Zhang, K.; Guan, G.; Liu, B.; Wang, S.; Zhang, Z. *Chem. Comm.* **2010**, *46*, 7319.